energies

MDPI

Article

Using Finite Element Method for Stress-Strain Evaluation of Commonly Used Buried Pipelines in Fault

Ning Tan [1,*], Liang Zhou [2], Weibo Zheng [2], Honglin Song [2], Zhibin Sun [1], Zhiyin Wang [1], Guisheng Wang [2], Guanjun Wang [2], Liming Zhang [3,*] and Xingyu Zhou [3]

[1] Sinopec, Beijing 100000, China; sunzb@sinopec.com (Z.S.); wangzy@sinopec.com (Z.W.)
[2] Technical Inspection Center, Sionpec Group Shengli Oilfield Company, Dongying 257100, China; zhouliang.slyt@sinopec.com (L.Z.); zhengweibo.slyt@sinopec.com (W.Z.); songhonglin800.slyt@sinopec.com (H.S.); wanggsh.slyt@sinopec.com (G.W.); wangguanjun.slyt@sinopec.com (G.W.)
[3] School of Petroleum Engineering, China University of Petroleum (East China), Qingdao 266580, China; s20020123@s.upc.edu.cn
* Correspondence: tanning@sinopec.com (N.T.); zhangliming@upc.edu.cn (L.Z.)

Abstract: In different kinds of buried pipelines, L245 and L360 are the most used which are chosen by the China Pipeline Design Institute. For studying the stress and deformation characteristics of buried pipelines with different specifications across faults, this paper established a physical model of cross-fault buried pipelines and a finite element model of pipelines crossing the fault zone, which adopts the finite element method and ANSYS software. The models take pipeline material, soil material, grid division, load application method, and other factors into consideration, concentrating on the nonlinear solution of L245 and L360 buried pipelines under the condition of strike-slip fault soil. The results illustrate that pipelines with larger diameters are more conducive to resisting the stress and deformation caused by faults. Moreover, the strain and dislocation amount of the pipeline increases with the increase of the dislocation amount when a fault occurs. Furthermore, the resistance is optimal when the angle of intersection between the fault and the pipe is 60, while further research and analysis are needed for special cases. This work can provide a direction for the optimization of parameters for pipeline design especially strain-based design.

Keywords: buried pipeline; finite element method; fault; contact stiffness; dislocation

Citation: Tan, N.; Zhou, L.; Zheng, W.; Song, H.; Sun, Z.; Wang, Z.; Wang, G.; Wang, G.; Zhang, L.; Zhou, X. Using Finite Element Method for Stress-Strain Evaluation of Commonly Used Buried Pipelines in Fault. *Energies* **2022**, *15*, 1655. https://doi.org/10.3390/en15051655

Academic Editor: José A. F. O. Correia

Received: 28 January 2022
Accepted: 21 February 2022
Published: 23 February 2022

1. Introduction

Refined oil distribution is a significant part of the process for consumers getting oil, and long-distance pipelines are an important guarantee for refined oil distribution [1,2]. Most of the long-distance pipelines in our country pass through active geological fault zones, and frequent geological activities near fault zones pose a great threat to the normal operation of underground pipelines that cross faults [3]. Current research shows that the causes of earthquake damage to buried pipelines can be divided into two categories: one is strong ground movement; the other is permanent ground deformation, such as site damage caused by fault movement, sand liquefaction, landslides, etc., [4]. Among them, the biggest impact on buried pipelines is the surface rupture caused by fault movement. Among them, the nature of the fault, site conditions, embedding methods, pipeline materials, and other factors have a significant impact on the degree of damage caused by fault movement. Therefore, it is of great significance to study the mechanical properties of buried pipelines in fault movement.

At present, the theoretical analytical method and finite element analysis method are two mainstream methods used to study the stress and strain analysis of pipelines. Theoretical analytical methods generally simplify the thin shell structure of pipelines into cable or beam models before theoretical calculation. Although the theoretical analytical

model can obtain accurate analytical solutions, it is difficult to apply to solve engineering problems with more complex conditions.

The reaction analysis method of buried pipelines in fault was first proposed by N. M. Newmark and his student W. J. Hall in 1973 [5]. They come up with a three-broken-line model. In 1977, based on the Ramberg–Osgood stress-strain model, Kennedy derived a new formula of strain and its functional form as [6]:

$$\varepsilon(\sigma) = \frac{\sigma}{E}\left[1 + \left(\frac{\alpha}{r+1}\right) \cdot \left(\frac{|\sigma|}{\sigma_y}\right)\right]^r \quad (1)$$

Then in 1985, Leon Ru-Liang Wang brought forward an improved method, which considered the bending strain and stiffness [7].

So far, the numerical analysis method of the finite element model has been used more widely than the stress and deformation analysis of pipelines. The finite element method can be roughly divided into two categories: one is to divide the pipeline into beam elements, which is relatively simple; the other divides the pipe into shell units. In both of these finite element methods, soil springs connected in three directions are used to consider the interaction between pipes and soil [8,9]. Zhang Kun et al. used the calculation model of pipe plastic deformation to analyze and calculate the pipe plastic deformation under the action of radial extrusion and residual pressure of pipe leakage to calculate the required load amount of pipe extrusion [10]. Wang Lei, Xie Qiang et al., Liu et al., and Shang Yujie et al., based on the elastic foundation beam model, derived the analytical solution of pipeline deformation and internal force under the action of a transverse landslide and studied the characteristics of pipeline deformation by the finite element simulation method. Chen Liqiong and Xue Jinghong used numerical simulation software to analyze the stress and strain distribution of buried pipelines crossing landslides, and studied the effects of soil properties, pipe diameter, wall thickness, internal pressure and pipe material on the stress and strain of pipelines. The finite element method is often used to simulate the actual seismic damage and aseismic experiment of pipeline crossing fault.

In this paper, the influence of a strike-slip fault on a buried pipeline is analyzed by the finite element model.

2. Finite Element Analysis Model

According to Saint-Venant's principle, the phenomenon of stress concentration generally appears near the point where the object is subjected to force. However, after a certain distance from the point of application of the force, the stress distribution tends to be uniform, that is, the local load of the object only affects a relatively small area near it, and the local effect of uneven stress can be ignored at a longer distance [11]. In this working condition, the large deformation of the pipe soil is mainly concentrated in a certain range on both sides of the fault, and the pipe section far away from the fault will move with the soil. On the premise of ensuring the safety of the large-deformation pipe section near the fault, the site with a small possibility of distal failure may not be analyzed.

Based on the above analysis, first, a physical model for analyzing buried pipelines across faults is established. As shown in Figure 1, the length, width, and height of the soil are 60 m, 20 m, and 10 m, respectively, the length of the pipeline is 60.2 m, and the center axis of the pipeline is 10 m from both sides of the soil.

This section can be divided by subheadings. It should provide a concise and precise description of the experimental results, their interpretation, as well as the experimental conclusions that can be drawn.

2.1. Material Parameter Setting

The stress-strain curves of pipes and soil materials are plastically nonlinear. When the strain exceeds the yield strain, the response of the material becomes nonlinear and irreversible. Under the action of a fault, the stress value of the pipeline may exceed the

yield stress and enter a nonlinear state; under the action of gravity and the shearing action of the pipeline, the faulted soil may also enter the material nonlinear stage [12–14].

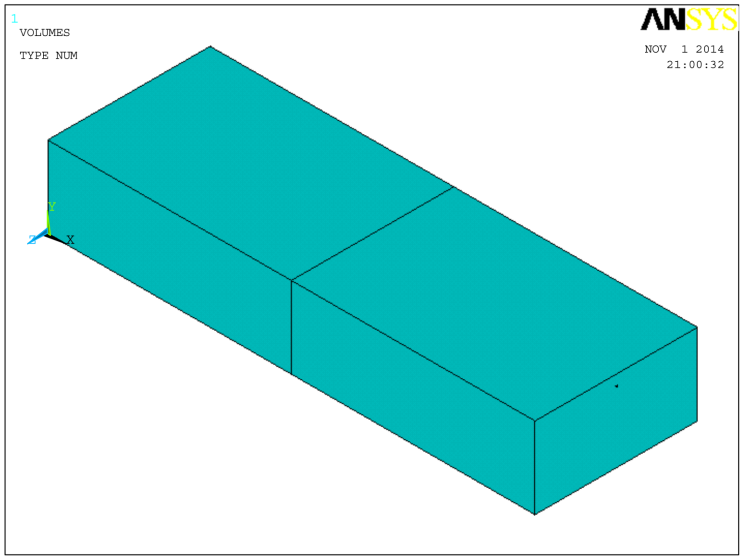

Figure 1. Physical model of buried pipeline across faults.

2.1.1. Pipe Material

According to the recommendations of SY/T 0450-2004 "Code for Seismic Design of Buried Oil (Gas) Steel Pipelines", the stress-strain curve of pipeline steel adopts a three-fold line model, which is divided into an elastic zone, an elastoplastic zone, and a plastic zone [15,16].

Two factors are considered. The grid division result of the faulted soil model is shown in Figure 2.

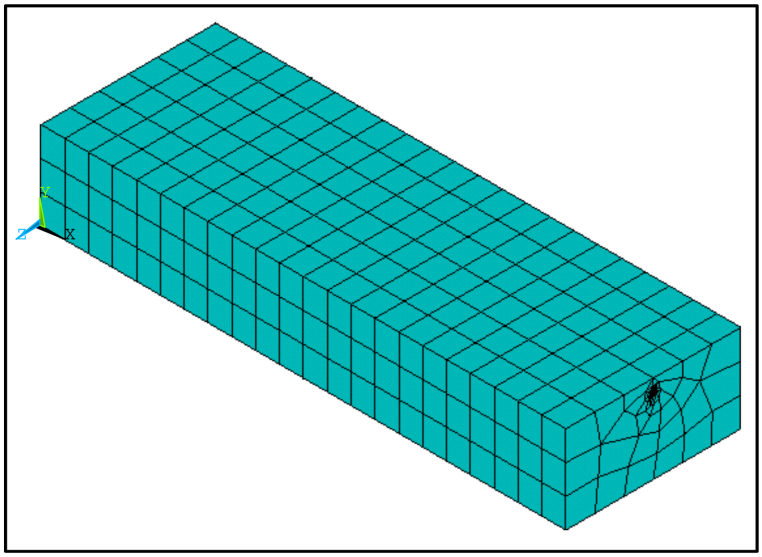

Figure 2. Grid division of faulted soil.

When meshing in ANSYS, it is stipulated that when meshing complex surfaces, each element edge at the curved edge should not exceed 15°, otherwise inverse elements will be generated here, which will cause analysis errors. Therefore, for the pipeline, at least 24 parts need to be divided on the circumference.

The finite element model of the cross-fault pipeline is shown in Figure 3. When dividing the mesh, divide the mesh along the pipe circumference and axial direction, and

divide the pipe circumference with 24 elements. When using ANSYS for structural analysis, try to avoid using lower-order tetrahedral elements, and use sweep division instead. For pipes, all hexahedral elements are generated.

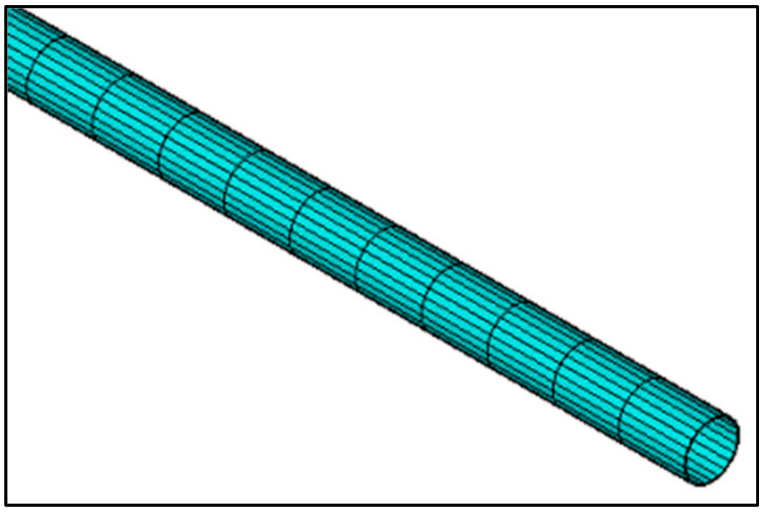

Figure 3. Grid division of pipelines laid across slopes.

The surface-to-surface three-dimensional contact pair establishes the finite element model of the pipeline crossing the fault zone, and also uses the SOLID45 element to simulate the pipeline and soil.

2.1.2. Soil Materials

The constitutive relationship of the soil is ideal elastoplastic, that is, after the equivalent stress reaches the yield limit, the stress will no longer increase, however, the strain will continue to increase. Use the Drucker–Prager model that comes with the ANSYS software to define the soil material, the equation is [17]:

$$f(I_1, J_2) = \alpha I_1 + \sqrt{J_2} - K = 0, \quad (2)$$

where I_1 is first invariant of stress tensor; and J_2 is second invariant of stress deviator tensor. α and K depend on three parameters: cohesion c, internal friction angle φ, and expansion angle ψ.

2.2. Meshing

Meshing is an important step for finite element analysis, and it directly affects the accuracy of the calculation results. In general, the greater the mesh density, the better the convergence of the calculation results and the higher the calculation accuracy, however, the calculation time is longer. Therefore, when determining the number of meshes, it is necessary to weigh the contact unit CONTA174 and the target unit TARGE170 to form a surface-surface three-dimensional contact pair.

Since the pipe has a much higher stiffness relative to the soil, the contact problem is rigid to flexible. The outer surface of the pipeline is the target surface, and the interface between the faulted soil and the pipeline is the contact surface, and the two together form a contact pair. The properties of the two faulted soils are the same, and one of the contact surfaces is selected as the target surface and the other is the contact surface, forming a contact pair.

For the surface-to-surface contact unit, the contact algorithm uses the augmented Lagrangian algorithm. At the beginning of the iteration, the contact coordination condition is determined by the penalty stiffness coefficient FKN. Once the balance is reached, the permissible intrusion amount is checked. At this time, if necessary, increase contact stress

to reduce the amount of intrusion. The advantage of this method is that it is not easy to cause pathological conditions, has less sensitivity to contact stiffness, and can better meet the real conditions of non-invasiveness. However, the disadvantage is that it requires more iterations and consumes more computing resources [18].

The amount of penetration between the two surfaces depends on the contact stiffness. In theory, the greater the contact stiffness, the smaller the penetration, which is more in line with the real situation. However, too much contact stiffness may cause the ill-condition of the total stiffness matrix, resulting in difficulty in convergence. In this paper, the normal stiffness coefficient FKN is set to 0.1, and the maximum contact penetration tolerance FTOLN is set to 0.1. To improve convergence, we turn on the automatic reduction of initial penetration.

In ANSYS, the friction between the target surface and the contact surface adopts the Coulomb model, and there are additional options to deal with complex adhesion and shear behavior. Before the two surfaces begin to slide relative to each other, the shear stress on the two surfaces must rise to a fixed value τ, and this stage is called adhesion. Once the shear stress exceeds this value, the two surfaces will slide relative to each other. The pipe–soil friction coefficient is selected concerning "Strength Design of Pipelines and Storage Tanks".

Considering that the pipe–soil contact problem involves friction, the stiffness matrix chooses the asymmetric option. Although the asymmetric solver requires more calculation time than the symmetric solver, for cross-fault problems, the friction stress has a greater influence on the calculation results, and the magnitude of the friction stress is highly dependent on the solution process and has any effect on the stiffness matrix. Symmetrical approximation may lead to reduced convergence.

In summary, the pipe–soil interaction is simulated by setting up contact pairs between the pipe and the soil, and between the soil and the soil. The contact pair model is shown in Figure 4.

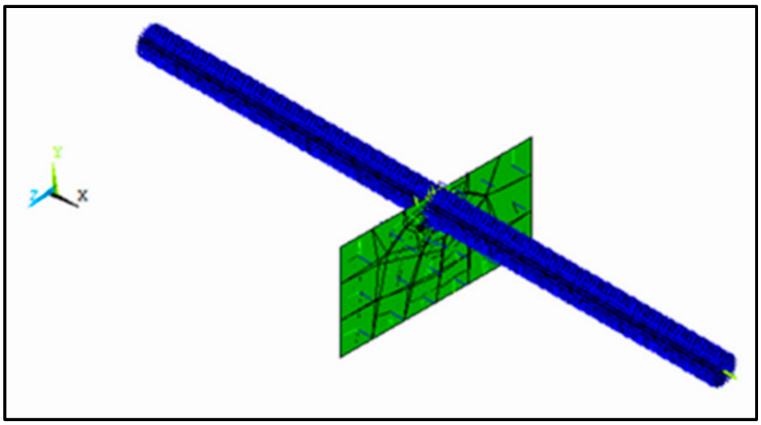

Figure 4. Contact pair model.

2.3. Boundary Conditions and Load Application

In the beam or shell finite element method, the interaction between the tube and the soil is considered by the axial soil spring and the transverse soil spring (including the horizontal soil spring and the vertical soil spring) connected to the node of the tube element, as shown in Figure 4. Since the fault displacement may be very large, the nonlinear characteristics of the soil spring must be considered. The parameters of the axial soil spring are determined by the backfill in the trench, while the parameters of the lateral soil spring (including the horizontal and vertical soil springs) are determined by the soil conditions around the pipeline buried site. In addition, when the pipeline moves in the vertical plane, due to the surface soil having an empty surface, the stiffness of the foundation soil of the pipeline upward and downward is different, that is, the soil reaction force and downward displacement of the pipeline relative to the soil. The soil reaction force of displacement is different [19–21].

When strike-slip faults slip, cross-fault pipelines will be subjected to shear, bending, tension and compression forces, resulting in tensile, compression, or buckling failure. When a strike-slip fault occurs in an earthquake, it can be regarded as a large displacement of the soil on one side, and no change in the geometric boundary of the soil on the other side. Therefore, the bottom surface of the soil on one side is fully constrained, the degrees of freedom in the three directions are set to 0, and the normal displacements of several sides perpendicular to the bottom surface are restrained at the same time. The degree of freedom in the two directions of X and Y is 0.

The gravity load in ANSYS is applied in the form of inertial force; therefore, the direction of the gravity acceleration g is in the positive direction of the Y-axis. In addition, internal pressure is applied to the inner surface of the pipe. The schematic diagrams of boundary conditions and load application are shown in Figures 5 and 6.

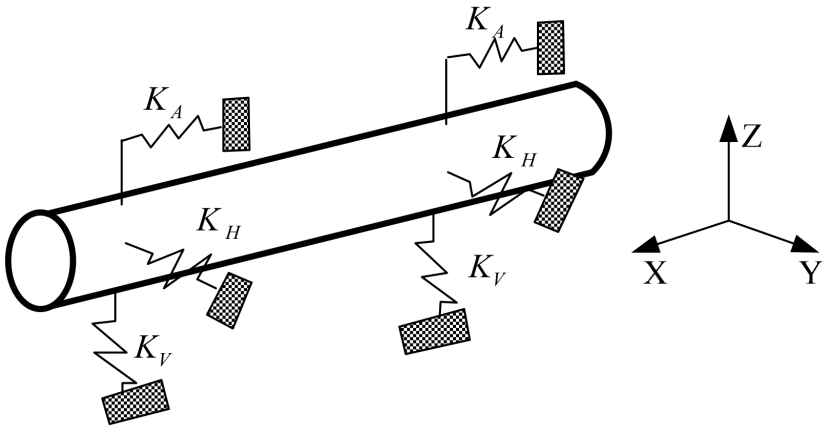

Figure 5. Finite element analysis diagram of buried pipeline.

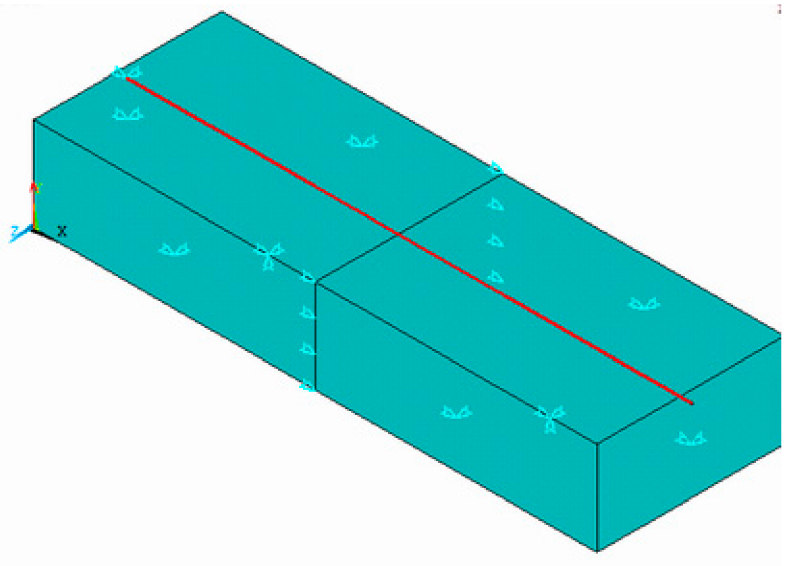

Figure 6. Schematic diagram of boundary conditions and load application.

3. Simulation Result Analysis

3.1. Stress and Strain Cloud Diagram

We performed nonlinear solutions to the established finite element model and performed post-processing on the calculation results. Figures 7 and 8 are the stress and strain cloud diagrams of the pipe section near the fault. It can be seen that under the action of the faulted soil, the pipe section near the fault will produce greater stress deformation.

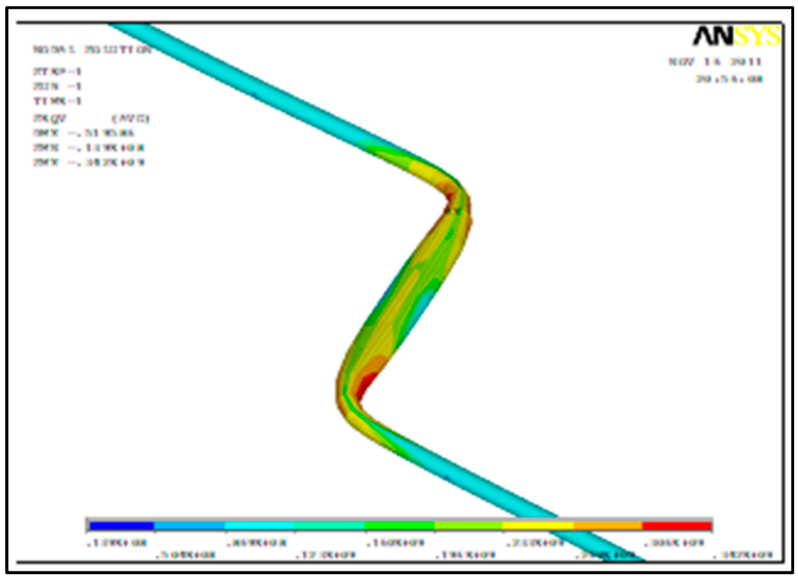

Figure 7. Stress cloud diagram of the pipe section near the fault.

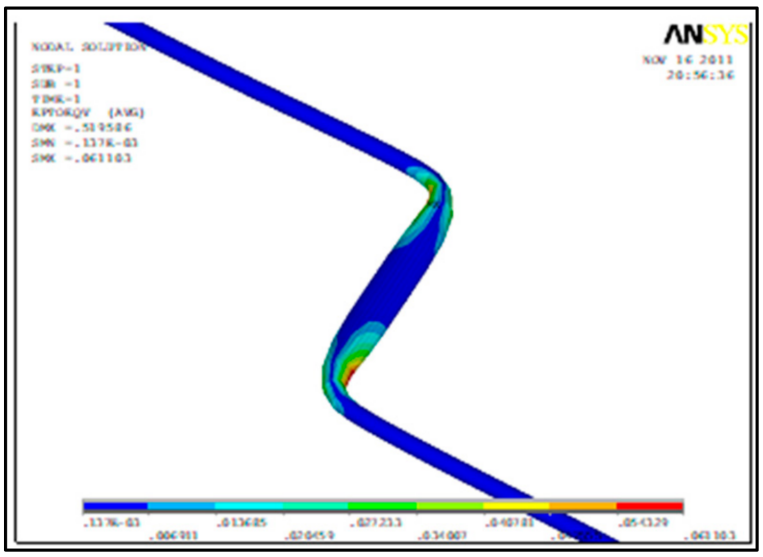

Figure 8. Strain cloud diagram of the pipe section near the fault.

In this paper, a total of 24 types of buried pipelines with different diameters and wall thicknesses of L245 and L360 are simulated and analyzed by the finite element method. The simulation results of L360 323.9 × 8.5 buried pipelines are used as an example for analysis. Figures 9–11 show the displacement, stress, and strain clouds of this size pipe when the dislocation occurs in the fault, respectively. As shown in Figure 9, the buried pipeline is shifted significantly with the fault dislocation, and significant bending deformation occurs on both sides of the fault. Figure 10 shows that when the fault is dislocated, the bent pipe section near the fault generates higher stress, and as shown in Figure 11, the bent pipe section near the fault then generates larger strains and contains larger plastic strains with similar distribution characteristics as the stress. Through the above cloud analysis, it can be seen that when dislocation occurs in the fault, the buried pipeline across the fault will be followed by a large displacement, and the pipeline on both sides of the fault will be bent and deformed, and a large stress-strain will be generated in the bent pipe section.

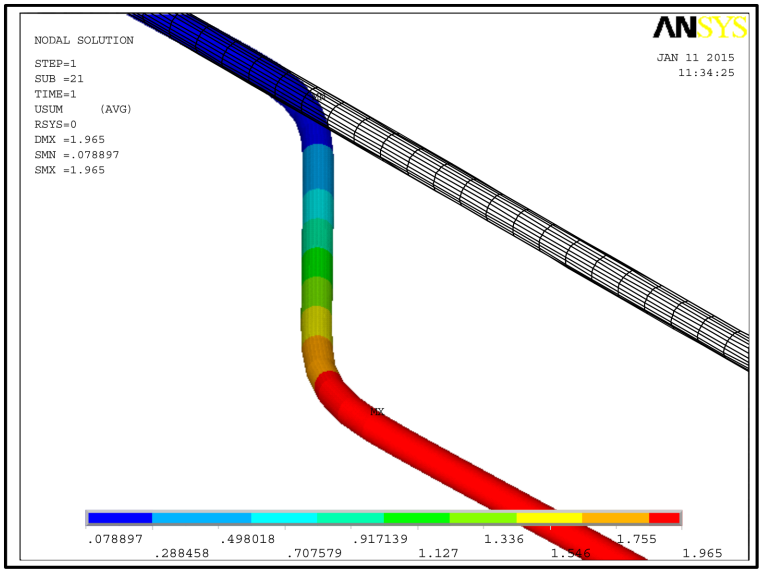

Figure 9. Pipeline displacement cloud diagram.

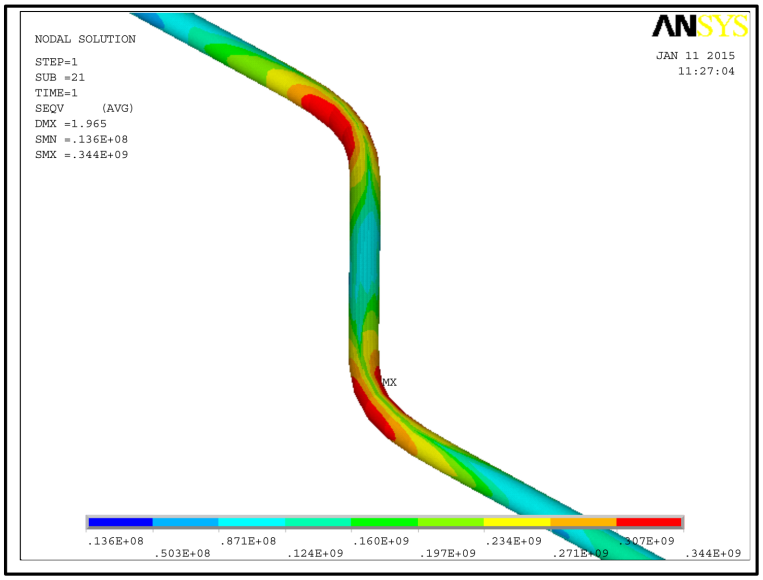

Figure 10. Pipeline stress cloud diagram.

3.2. Stress and Strain Cloud Diagram

In the series simulation analysis of buried pipeline across the fault, it is assumed that the soil is hard clay, and according to the Petroleum and Chemical Engineering Design Workbook Book 2 Oilfield Surface Engineering Design, the soil physical parameters used are shown in Table 1; according to GB/T17395-2008 Seamless Steel Pipe Size, Profile, Weight and Allowable Deviation, the pipe specification parameters used are shown in Table 2. In Table 2, because of the required toughness of pipelines, L245 and L360 are chosen as the pipe material. The chosen diameters are the most commonly encountered in the work of a pipeline design institute in China.

Table 1. Physical parameters of soil.

Soil Type	Modulus of Elasticity /MPa	Density/kg/m^3	Poisson's Ratio	Cohesion/MPa	Internal Friction
Stiff Clay	10	1800	0.15	0.06	56

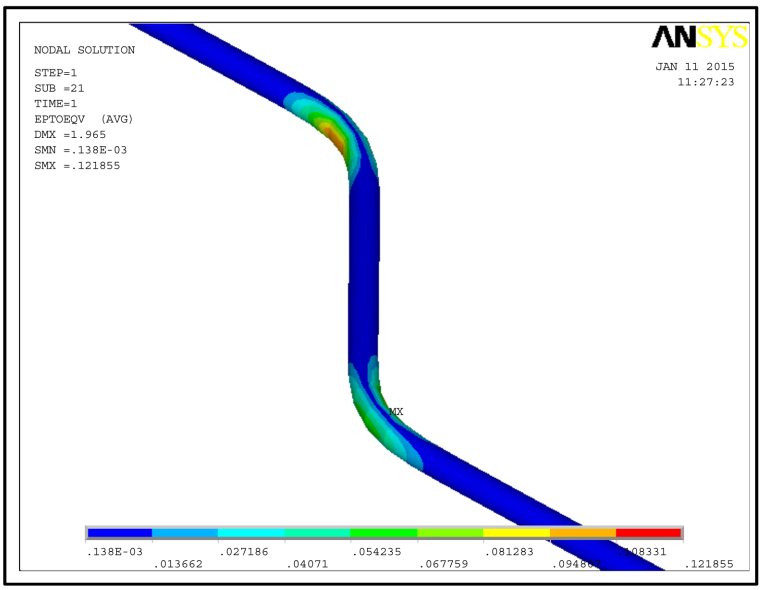

Figure 11. Pipeline strain cloud diagram.

Table 2. Pipeline specifications.

Model	Number	Diameter/mm	Wall Thickness/mm
L245	111 112 113 114	168.3	4.5 5.0 5.5 6.0
L245	121 122 123 124	219.1	6.0 6.3 7.0 7.5
L245	131 132 133 134	323.9	7.1 7.5 8.0 8.5
L360	211 212 213 214	168.3	4.5 5.0 5.5 6.0
L360	221 222 223 224	219.1	6.0 6.3 7.0 7.5
L360	231 232 233 234	323.9	7.1 7.5 8.0 8.5

We use the selected initial data to simulate and analyze the buried pipeline in the process of fault dislocation, and the relationship between the maximum strain of the L245 series pipeline and the amount of fault dislocation is organized according to the calculation results as follows:

According to Figure 12, it can be seen that the pipe strain shows a complex nonlinear relationship with the amount of dislocation when dislocation occurs in the fault, which can be roughly distinguished into two regions: (1) the strain increases with the amount of

dislocation; (2) the strain oscillates with the increasing amount of dislocation. The cut-off value of the two regions varies depending on the pipe specification and the intersection angle between the pipe and the fault. Among the four pipe sizes, 323.9 × 7.1 pipe has the best ability to resist dislocation at an intersection angle of 30°, followed by 90° and the worst at 60°; the other three pipe sizes have the best intersection angle with the fault at 60°, followed by 90° and the worst at 30°.

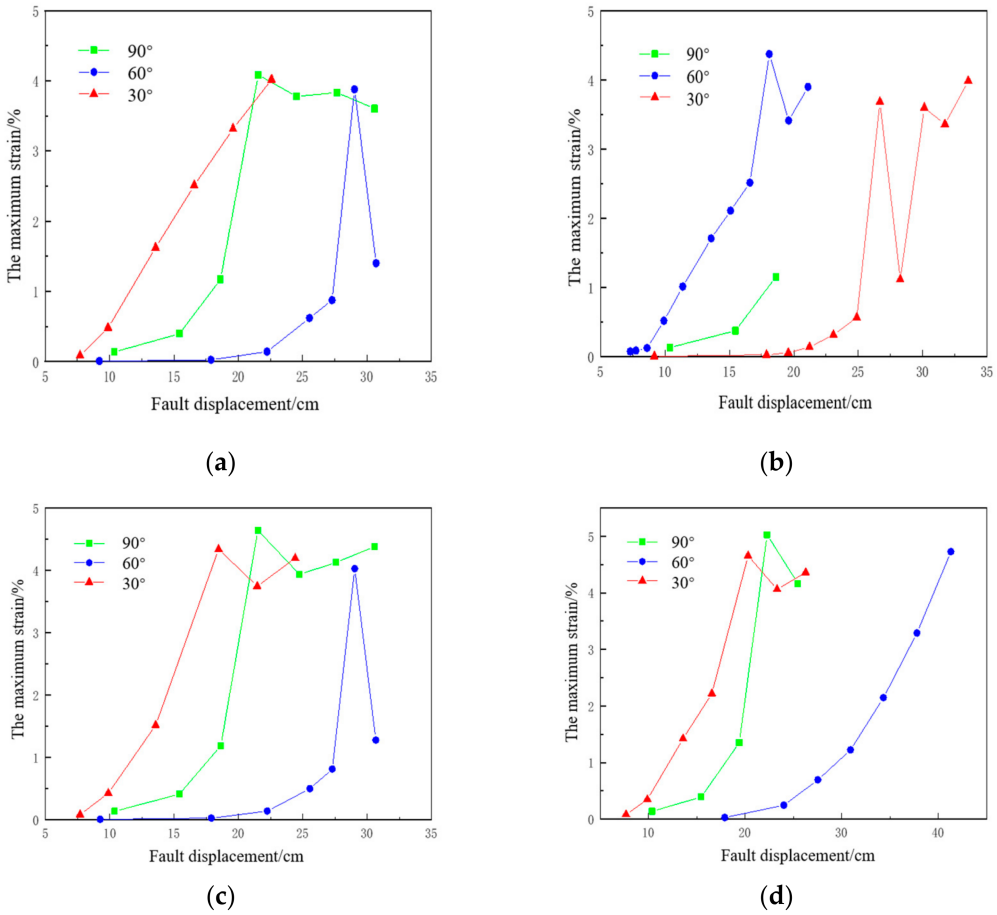

Figure 12. The maximum strain change law of pipeline under different included angles: (**a**) 323.9 × 7.1; (**b**) 323.9 × 7.5; (**c**) 329.9 × 8.0; (**d**) 329.9 × 8.5.

According to Figure 13, the strain of the pipe and the amount of dislocation when the fault occurs show a complex non-linear relationship, but the strain increases with the increase in the amount of dislocation and the trend of increasing. Among the four pipe specifications, 219.1 × 6.0 pipe in the intersection angle of 30° when the best ability to resist dislocation, 90° followed by the worst 60°; the other three specifications of the pipe and the intersection angle of the fault are the best 60°, 90° followed by the worst 30°.

According to Figure 14, various sizes of pipes require fault dislocations of about 20 cm at 60° intersection angle before significant strain occurs, but the 90° intersection angle and 30° intersection angle change significantly after greater than 10 cm of fault dislocations.

The relationship between the maximum strain and the amount of fault dislocation for the L360 series pipeline simulated in our work is shown in Figures 15–17. It can be seen that the L360 series pipe behaves similarly to the L245 series, and the strain of the pipe shows a complex non-linear relationship with the amount of dislocation when dislocation occurs in the fault, but the strain tends to increase with the increase of the amount of dislocation. Among the four pipe specifications, all three pipes have the best ability to resist dislocations at an intersection angle of 60° with the fault, followed by 90° and the worst at 30°.

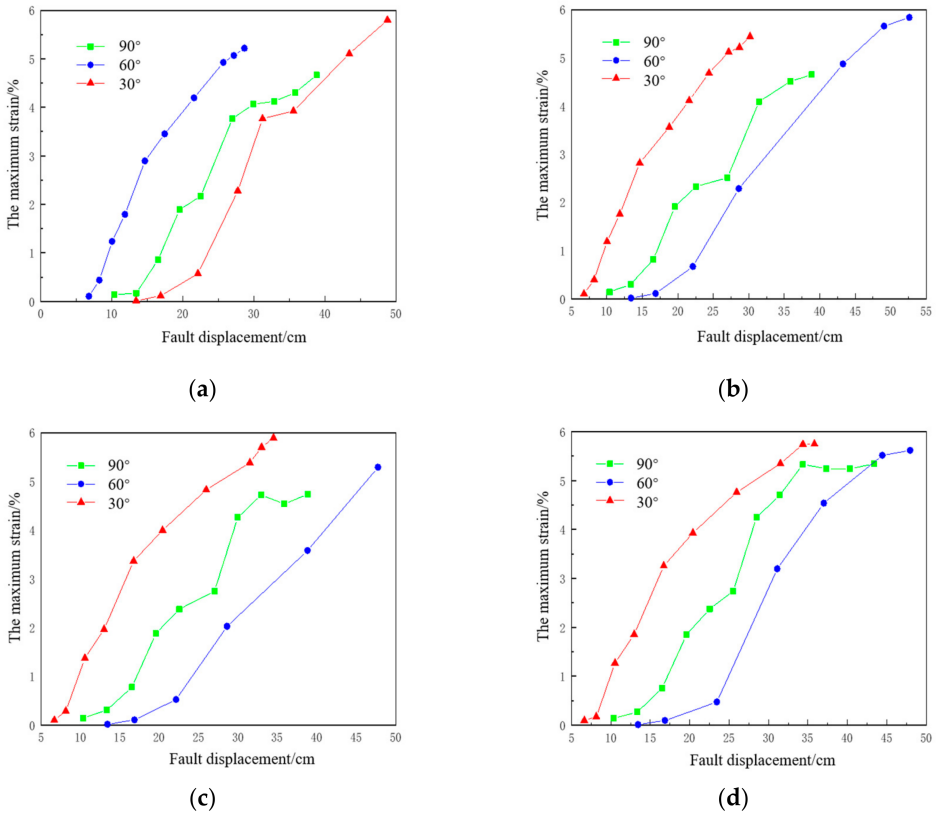

Figure 13. The maximum strain change law of pipeline under different included angles: (**a**) 219.1 × 6.0; (**b**) 219.1 × 6.3; (**c**) 219.1 × 7.0; (**d**) 219.1 × 7.5.

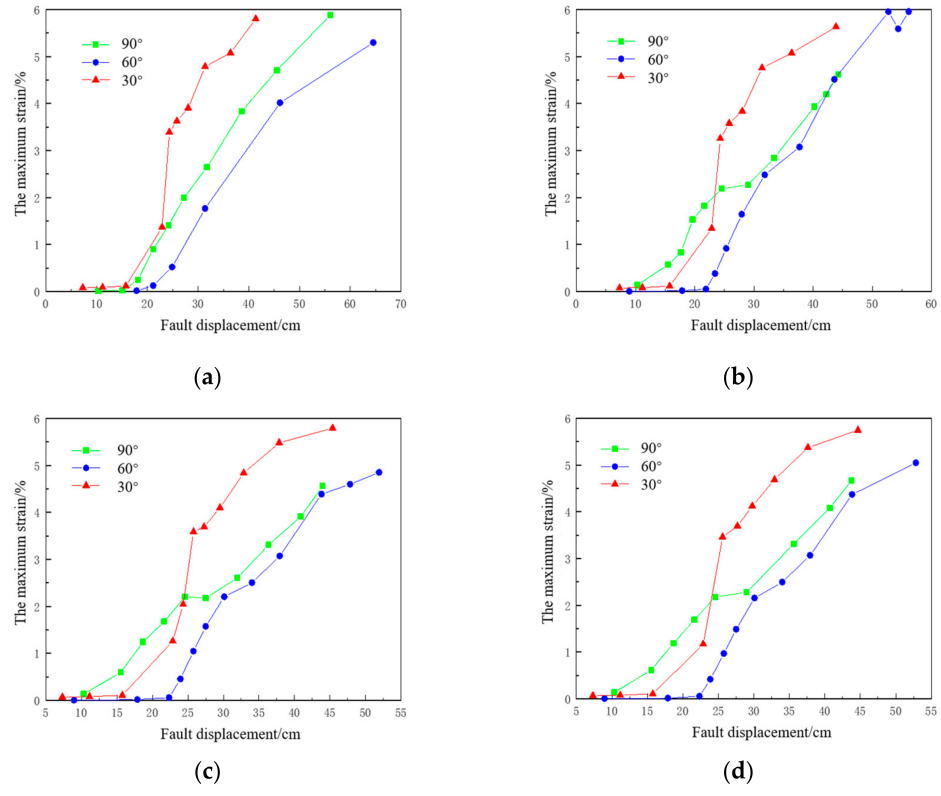

Figure 14. The maximum strain change law of pipeline under different included angles: (**a**) 168.3 × 4.5; (**b**) 168.3 × 5.0; (**c**) 168.3 × 5.5; (**d**) 168.3 × 6.0.

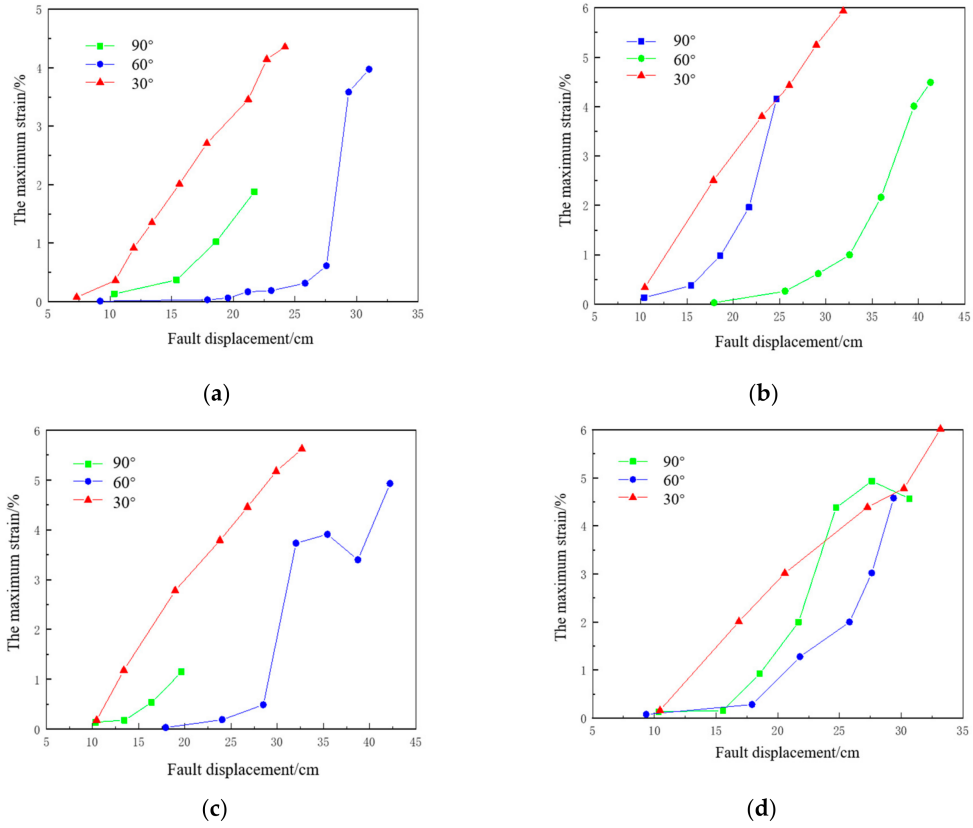

Figure 15. The maximum strain change law of pipeline under different included angles: (**a**) 323.9 × 7.1; (**b**) 323.9 × 7.5; (**c**) 323.9 × 8.0; (**d**) 323.9 × 8.5.

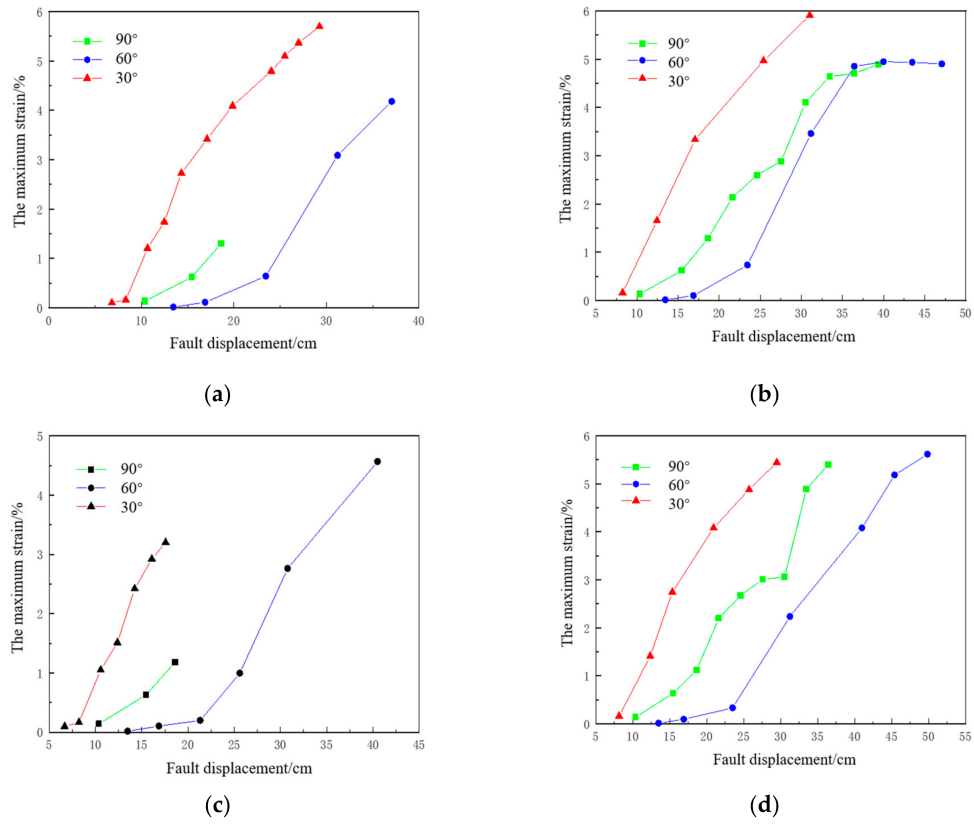

Figure 16. The maximum strain change law of pipeline under different included angles: (**a**) 219.1 × 6.0; (**b**) 219.1 × 6.3; (**c**) 219.1 × 7.0; (**d**) 219.1 × 7.5.

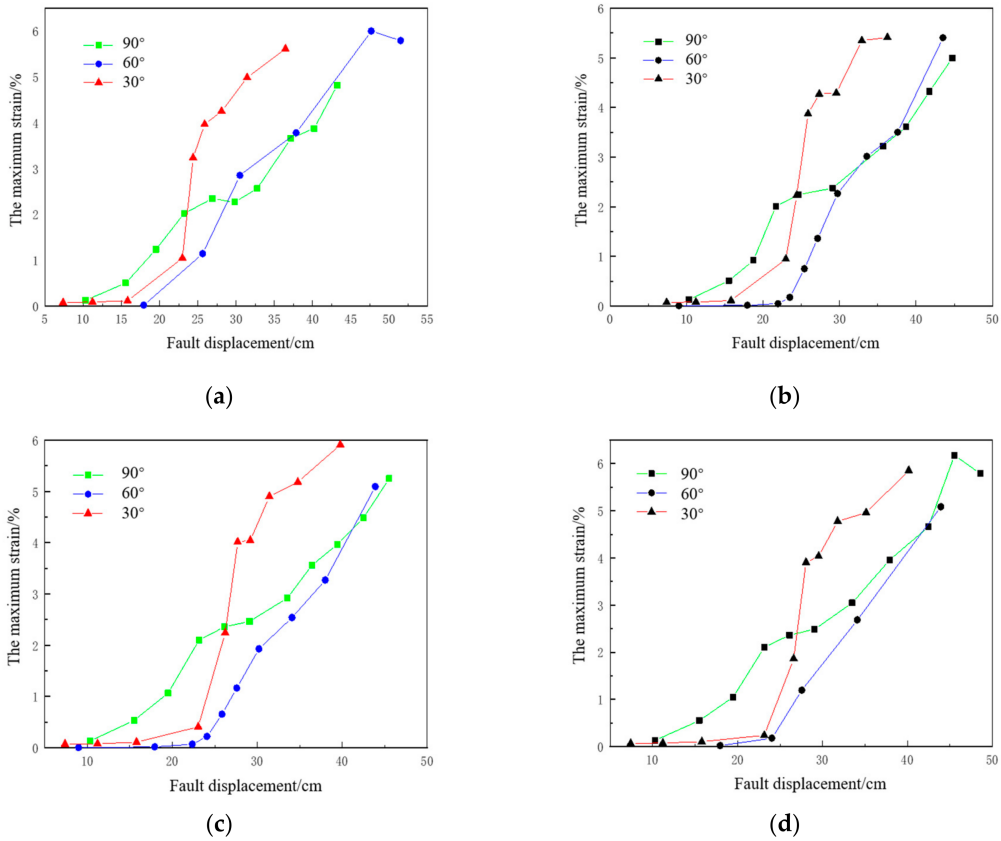

Figure 17. The maximum strain change law of pipeline under different included angles: (**a**) 168.3 × 4.5; (**b**) 168.3 × 5.0; (**c**) 168.3 × 5.5; (**d**) 168.3 × 6.0.

4. Conclusions

In our work, ANSYS was applied to test and analyze different sizes of buried pipelines for the effects of slip faults, and the following conclusions were drawn:

Each pipe has a strain threshold. The pipe strain with the increase in the amount of fault dislocation changes very little when the amount of fault dislocation is less than the threshold. Moreover, the pipe strain with the increase in the amount of dislocation and the increasing trend will rapidly increase when the amount of fault dislocation is greater than the threshold. Therefore, the maximum strain of buried pipes should be less than this point in engineering applications.

The pipeline strain and dislocation amount show a complex non-linear relationship when dislocation occurs in the fault, but basically, the strain increases with the increase of the dislocation amount. Especially, after the strain of L245 pipe increases to a certain range with the increase of dislocation amount, the strain will oscillate and change with the increase of dislocation amount, the critical value of which varies with the pipe specification and the intersection angle between the pipe and the fault, and further analysis and test are needed.

Generally, the resistance ability of the intersection angle between the fault and the pipe is optimal at 60°, and the resistance ability of the intersection angle between the fault and the pipe is the worst at 90°. In particular, the L245 model 323.9 × 7.1 pipeline has the worst resistance at 60°, and the best resistance at 30°. The same special one is the L245 model 219.1 × 6 pipeline, whose law is the same as the L245 model 323.9 × 7.1 pipeline.

A larger pipe diameter is more conducive to resisting the stress deformation caused by the fault.

The above results are mainly used for "strain-based pipeline design" and the parameter optimization of pipelines.

Author Contributions: Conceptualization, N.T. and L.Z. (Liang Zhou); methodology, N.T.; software, L.Z. (Liang Zhou), W.Z., H.S. and Z.S.; validation, N.T., Z.W.; formal analysis, L.Z. (Liang Zhou); investigation, Z.W.; resources, L.Z. (Liming Zhang); data curation, L.Z. (Liming Zhang); writing—original draft preparation, L.Z. (Liang Zhou); writing—review and editing, X.Z.; visualization, G.W. (Guisheng Wang); supervision, G.W. (Guanjun Wang); project administration, L.Z. (Liming Zhang); funding acquisition, N.T. All authors have read and agreed to the published version of the manuscript.

Funding: This work is supported by the National Natural Science Foundation of China under Grant 51722406, 61573018, 52074340, and 51874335, the Shandong Provincial Natural Science Foundation under Grant JQ201808 and ZR2019MEE101, the Major Scientific and Technological Projects of CNPC under Grant ZD2019-183-008, the Science and Technology Support Plan for Youth Innovation of University in Shandong Province under Grant 2019KJH002, the National Science and Technology Major Project of China under Grant 2016ZX05025001-006, 111 Project under Grant B08028.

Institutional Review Board Statement: Not applicable.

Informed Consent Statement: Not applicable.

Data Availability Statement: Not applicable.

Acknowledgments: The authors would like to thank the Technical Inspection Center, SIONPEC Shengli Oilfield Company for their assistance in numerical simulation.

Conflicts of Interest: The authors declare no conflict of interest.

Abbreviations

FEA	Finite Element Method
ANSYS	A general calculation software
FKN	Penalty Stiffness Factor in ANSYS
FTOLN	Maximum Permeability Tolerance in ANSYS
SOLID45	Solid element parameter in ANSYS
CONTA174	Contact element parameter in ANSYS
TARGE170	Target surface element parameter in ANSYS

References

1. Xu, X.; Wang, C.; Zhou, P. GVRP considered oil-gas recovery in refined oil distribution: From an environmental perspective. *Int. J. Prod. Econ.* **2021**, *235*, 108078. [CrossRef]
2. Xu, X.; Lin, Z.; Li, X.; Shang, C.; Shen, Q. Multi-Objective robust optimisation model for MDVRPLS in refined oil distribution. *Int. J. Prod. Res.* **2021**, *21*, 1–21. [CrossRef]
3. Tsatsis, A.; Gelagoti, F.; Gazetas, G. Performance of a buried pipeline along the dip of a slope experiencing accidental sliding. *Geotechnique* **2018**, *68*, 968–988. [CrossRef]
4. Karamitros, D.K.; Bouckovalas, G.D.; Kouretzis, G.P. Stress analysis of buried steel pipelines at strike-slip fault crossings. *Soil Dyn. Earthq. Eng.* **2007**, *27*, 200–211. [CrossRef]
5. Newmark, N.M.; Blume, J.A.; Kapur, K.K. Seismic Design Spectra for Nuclear Power Plants. *J. Power Div.* **1973**, *99*, 287–303. [CrossRef]
6. Kennedy, R.P.; Chow, A.M.; Williamson, R.A. Fault movement effects on buried oil pipeline. *Transp. Eng. J. Am. Soc. Civ. Eng.* **1977**, *103*, 617–633. [CrossRef]
7. Wang, L.R.L.; Yeh, Y.-H. A refined seismic analysis and design of buried pipeline for fault movement. *Earthq. Eng. Struct. Dyn.* **1985**, *13*, 75–96. [CrossRef]
8. Nejad, A.F.; Alipour, R.; Rad, M.S.; Yahya, M.Y.; Koloor, S.S.R.; Petru, M. Using Finite Element Approach for Crashworthiness Assessment of a Polymeric Auxetic Structure Subjected to the Axial Loading. *Polymers* **2020**, *12*, 1312. [CrossRef] [PubMed]
9. Jalali, H.H.; Rofooei, F.R.; Attari, N.K.A.; Samadian, M. Experimental and finite element study of the reverse faulting effects on buried continuous steel gas pipelines. *Soil Dyn. Earthq. Eng.* **2016**, *86*, 1–14. [CrossRef]
10. Zhang, K.; He, Z.; Zheng, K.; Yuan, S. Experimental verification of anisotropic constitutive models under tension-tension and tension-compression stress states. *Int. J. Mech. Sci.* **2020**, *178*, 105618. [CrossRef]
11. Yu, G.Q.; Wang, F.; Du, G. Finite Element Analysis of Stamped Tees Stress in Directly Buried Heating Pipeline. *Appl. Mech. Mater.* **2013**, *405*, 997–1001. [CrossRef]
12. Wang, M.; Zhong, M.; Long, Y.; Ding, K.; Xie, X.; Ying, L. Study on Dynamic Strain Regularity and Influencing Factors of Shallow Buried Metal Pipe under Collapse Impact Load. *Shock Vib.* **2018**, *2018*, 8792564. [CrossRef]

13. Zhao, J.; Zhang, H.; Chen, J.; Wu, X.; Wang, Y.; Gao, D.; Liang, Y. Influence of Coil Current and Oil Film Thickness on Hopf Bifurcation of MLDSB. *Energies* **2022**, *15*, 848. [CrossRef]
14. Fadaee, M.; Farzaneganpour, F.; Anastasopoulos, I. Response of buried pipeline subjected to reverse faulting. *Soil Dyn. Earthq. Eng.* **2020**, *132*, 106090. [CrossRef]
15. Fahmy, M.W.; Namini, A.H. A survey of parallel nonlinear dynamic analysis methodologies. *Comput. Struct.* **1994**, *53*, 1033–1043. [CrossRef]
16. Zhao, H.Y.; Jeng, D.S.; Guo, Z.; Zhang, J.S. Two-Dimensional Model for Pore Pressure Accumulations in the Vicinity of a Buried Pipeline. *J. Offshore Mech. Arct. Eng.* **2014**, *136*, 042001. [CrossRef]
17. Avci, O.; Bhargava, A. Investigation of Uplift Pressures on a Drainage Shaft Using ANSYS SOLID185 Elements and Drucker–Prager Failure Criterion for the Surrounding Rock Stratum. *J. Perform. Constr. Facil.* **2020**, *34*, 04019083. [CrossRef]
18. Khair, J.A.; Jaswar, K.; Effendi, A.; Fitriadhy, A. Buckling Criteria for Subsea Pipeline. *J. Teknol.* **2015**, *74*, 1–4. [CrossRef]
19. Rasouli, H.; Fatahi, B. (Eds.) Effect of Burial Depth on Pipeline-Fault Rupture Interaction Mechanism and Mitigation Technique Using Geofoam Blocks. In *Challenges and Innovations in Geomechanics, Proceedings of the International Conference of the International Association for Computer Methods and Advances in Geomechanics, Turin, Italy, 5–8 May 2021*; Springer: Cham, Switzerland, 2021.
20. Tohidifar, H.; Jafari, M.K.; Moosavi, M. Downwards force—Displacement response of buried pipelines during dip–slip faulting in sandy soil. *Can. Geotech. J.* **2021**, *58*, 377–397. [CrossRef]
21. Yu, C.; Han, C.; Xie, R.; Wang, L. Mechanical behavior analysis of buried pipeline under stratum settlement caused by underground mining. *Int. J. Press. Vessel. Pip.* **2020**, *188*, 104212. [CrossRef]